Ceramics International xxx (xxxx) xxx–xxx

Contents lists available at ScienceDirect

Ceramics International

journal homepage: www.elsevier.com/locate/ceramint

Short communication

High-entropy carbide: A novel class of multicomponent ceramics

Jieyang Zhou[a], Jinyong Zhang[a,*], Fan Zhang[a,*], Bo Niu[a], Liwen Lei[a], Weimin Wang[a]

[a] State Key Laboratory of Advanced Technology for Materials Synthesis and Processing, University of Technology, Wuhan 430070, China

ARTICLE INFO

Keywords:
High-entropy
Carbide
Microstructure
Composition
Oxidation

ABSTRACT

In this work, an equi-atomic (Ti, Zr, Hf, Nb, Ta) C high-entropy carbide (HEC) powder was synthesized using spark plasma sintering (SPS), and its phase evolution, microstructure, composition and oxidation behaviour were investigated in detail. According to the results, pure face-centred cubic structured solid solution could be obtained at 1950 °C, with metallic atoms randomly placed in the metallic sublattice. Results also showed that HEC powder exhibited better performance with regards to oxidation resistance than its original components and acted as an indivisible entirety while undergoing oxidation under relatively lower temperatures. This reflected from the side that HEC powder was thermally more stable than its original components.

1. Introduction

Configuration entropy, as the driving force for stabilization within a certain temperature range, has been manoeuvred in several studies conducted on various structures for the fabrication of new materials. When this mixing entropy is adequately high, an entropy-stabilized structure is formed with a random occupation of cation sites. In addition, an unusual synergistic effect, called the high-entropy effect, is demonstrated with lattice deformation and reduced diffusion [1–5].

Recently, researchers have focused on high-entropy systems due to their unique compositions, microstructures and adjustable properties [6–8]. This was verified in the study of high-entropy alloys (HEAs). In contrast to traditional alloys, which are based on one or two principal elements, HEAs are originally defined as alloys comprising of at least five principal metal elements in equal or near-equal ratios [9–11]. As a result of the high-entropy effect, the formation of simple solid solutions rather than complex phases, such as intermetallic compounds, would be facilitated in HEAs [12,13], due to which HEAs display excellent physico-chemical properties and demonstrate a promising future for various engineering applications [14].

Previous studies have shown that similar to the situation in HEAs, high-entropy oxides (HEOs) having highly symmetric structures could be fabricated by deliberately incorporating five metal elements into a single lattice with random and homogeneous occupancy [15–18]. Instead of cohesive energy, the entropic contributions to the free energy promote thermodynamic stability at a given temperature. Besides, Gild et al. [19] synthesized a series of high-entropy metal diborides using high-energy ball milling and spark plasma sintering (SPS). These high-entropy borides exhibited a single-phase solid solution with a layered hexagonal structure, showing higher hardness and better oxidation resistance than the average performances of five individual metal diborides fabricated using identical fabrication processing.

Inspired by these pioneering studies in alloy communities and oxides, the entropy concept was extended to five-component carbides in this work. It was supposed that the Gibbs free energy could be utilized in the stabilization of new carbide phase, and the IV B and V B carbides could display entropy-stabilized forms of crystalline matter, which were also called high-entropy carbide.

In this work, the (Ti, Zr, Hf, Nb, Ta) C high-entropy carbide (HEC) powder was prepared using spark plasma sintering (SPS) and the samples were characterized in terms of elemental and phase composition, microstructure and oxidation resistance, to provide a detailed description of its unusual composition, microstructure and oxidation behaviour, as compared with its original components.

2. Material and methods

2.1. Synthesis

The commercially available TiC (Aladdin, 99.99%), ZrC (Aladdin, 99%), HfC (Aladdin, 99.5%), NbC (Alfa Aesar, 99%) and TaC (Aladdin, 99.5%) were used as the original components. The powder mixture of five carbides with equal molar ratio (labelled as 'Mixed powder') was obtained using wet ball-milling (GMJ/B, Xianyang JinHong General Machinery Co., Ltd., China) in polyethylene jars with agate balls and ethyl alcohol as the media for 24 h. The slurry was dried in a rotary evaporator at 65 °C and granulated through a 200-mesh sieve. For studies on the synthesis process of high-entropy ceramic powder

* Corresponding authors.
E-mail addresses: shs@whut.edu.cn (J. Zhang), zhfan@whut.edu.cn (F. Zhang).

https://doi.org/10.1016/j.ceramint.2018.08.100
Received 25 July 2018; Received in revised form 8 August 2018; Accepted 10 August 2018

(labelled as 'HEC powder'), the obtained five-component mixed powder (Mixed powder) was subjected to a heat treatment in the spark plasma sintering (SPS, Dr. Sinter-3.20MK II, Sumitomo Coal Mining Co., Ltd., Japan) in vacuum (20 Pa) at the desired temperature for 5 min. The obtained powder samples were then hand-ground in an agate mortar to 200 mesh for subsequent experiments. The experiments were conducted sequentially at the temperatures of 1000 °C, 1100 °C, 1200 °C, 1300 °C, 1400 °C, 1500 °C, 1600 °C, 1700 °C, 1800 °C, 1900 °C, and 1950 °C, and the heating rate was 200 °C/min. In order to avoid the influence of uniaxial pressure, a special 20-mm inner diameter cylindrical graphite die was adopted, which could be used without pressure. Additionally, the die was wrapped in a layer of graphite wool during the synthesis process for ensuring the temperature homogeneity.

2.2. Characterization

The crystal structure of the synthesized HEC powder was characterized using X-ray diffraction (XRD, Rigaku Ultima III) with Cu Kα radiation. A step size of 0.02° and a collection time of 0.3 s at 40 kV and 40 mA over the diffraction angle (2θ) range of 10–90° were used. The lattice parameter of the sample was calculated according to Bragg equation based on the XRD data and the interplanar spacing equations about the FCC phase.

The microstructures of specimens were observed using scanning electron microscopy (SEM, Hitachi 3400). The structural and chemical analysis on the local scale of the specimens were conducted using transmission electron microscope (TEM, FEI Titan Themis 200), which was equipped with selected area electron diffraction (SAED) and energy dispersive spectrometer (EDS, Bruker Super-X).

In order to study the oxidation behaviours of Mixed powder and HEC powder, thermogravimetric analysis combined with differential scanning calorimetry (TG–DSC, Netzsch STA449F3, Germany) was used to perform an *in situ* thermogravimetric and calorimetric analyses under airflow using a heating rate of 10 °C/min.

For further study of oxidation processes, both Mixed powder and HEC powder were heated at desired temperature for 10 min in a muffle furnace (SX2-8-16, Wuhan DianLu Experimental Electric Furnace Factory) under air atmosphere. After the isothermal oxidation, the specimens were removed from the furnace and quenched down to room temperature. The specimens were then characterized using XRD with Cu Kα radiation to study their phase compositions. The experiments were conducted at the temperatures of 200 °C, 400 °C, 600 °C, 800 °C, 900 °C, 1200 °C and 1400 °C sequentially.

3. Results and discussion

3.1. Microstructure and composition of HEC powder

Fig. 1a displays the XRD patterns of the synthesized products at some representative temperatures. Furthermore, the diffractogram of Mixed powder is also shown in Fig. 1a for comparison. The results show that a single-phase solid solution with an FCC structure was gradually formed with the increase in temperature, and HEC powder was finally synthesized at 1950 °C.

In the case of HEC powder, the formation of pure FCC solid solutions was anticipated, because each of its five components have an FCC structure. It should also be noted that the synthesized HEC powder did not exhibit any preferred orientation. In comparison to TiC, the multi-component HEC powder exhibited a shift of XRD peak to lower angles, which was due to the presence of metallic elements (Zr Hf Nb Ta) with higher atomic radii than the Ti. It was interesting to compare the lattice parameter of HEC powder with those of the five binary carbides. With regards to HEC powder, the measured lattice parameters ***a*** had the value of around 4.5084 Å, whereas the calculated average value of the lattice constants of TiC, ZrC, HfC, NbC and TaC phases, as received from the JCPDS files, was 4.5125 Å. The small differences between the measured and calculated lattice parameter values supported the assumption that the metallic atoms were randomly placed within the metallic sublattice [10].

Fig. 1b presents the SEM images of HEC powder synthesized using SPS. The results confirmed the presence of spherical particles along with cuboidal particles of approximately 2 μm in size. Further TEM analysis along with the corresponding selected area electron diffraction (SAED), as demonstrated in Fig. 1c, proved the existence of pure FCC phase and the homogeneity of the solid-solution phase. The high-angle annular dark-field signal (HAADF) image is presented in Fig. 2a. In Fig. 2b–f, the EDS signals for the Kα emission energies of Ti, Zr, Hf, Nb and Ta are presented, indicating chemically and structurally homogeneous material.

Both the XRD and STEM–EDS analyses supported homogenous mixing, and therefore, it was concluded with satisfactory certainty that the (Ti, Zr, Hf, Nb, Ta) C HEC was successfully synthesized as a chemically and structurally homogeneous material with the metallic atoms randomly placed in the metallic sublattice. Based upon these results, the schematic diagram of the atomic configuration in the sublattice of (Ti, Zr, Hf, Nb, Ta) C HEC is presented in Fig. 2g, in which M, N, O, P and Q represent the metallic atoms (Ti, Zr, Hf, Nb, Ta) and C represents the carbon atom. It is worth noticing that this schematic exhibits only one possible situation and does not denote that the metallic atoms can only take the specific positions as shown in the sketch, which is due to the randomness of the arrangement of metallic atoms mentioned earlier. It should also be noted that this simplified schematic diagram does not take lattice distortion into consideration.

3.2. Oxidation behaviour of HEC powder

In order to compare the differences and similarities between the oxidation processes of Mixed powder and HEC powder, a

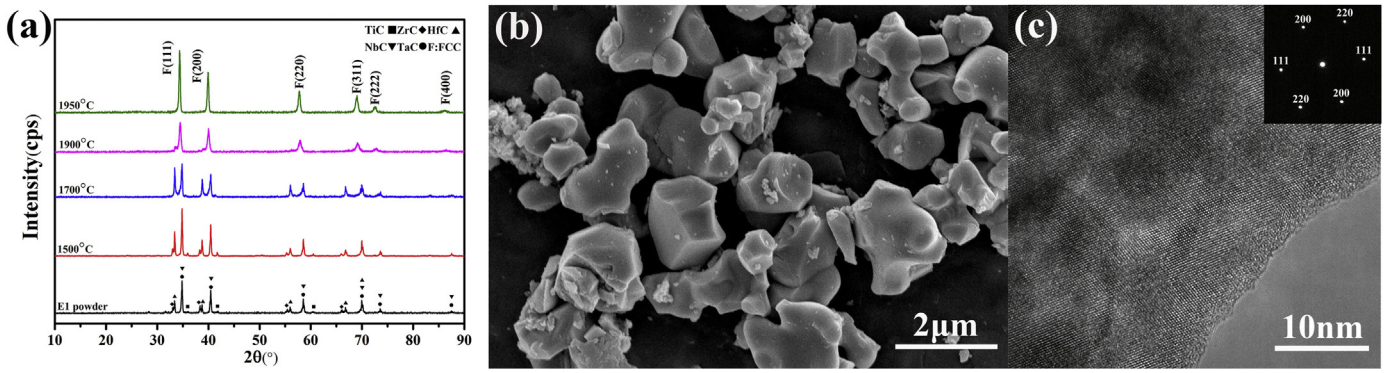

Fig. 1. (a) XRD patterns of synthesized products formed at 1500 °C, 1700 °C, 1900 °C and 1950 °C. (b) SEM images of HEC powder synthesized at 1950 °C. (c) TEM analysis of HEC powder and the corresponding selected area electron diffraction (SAED).

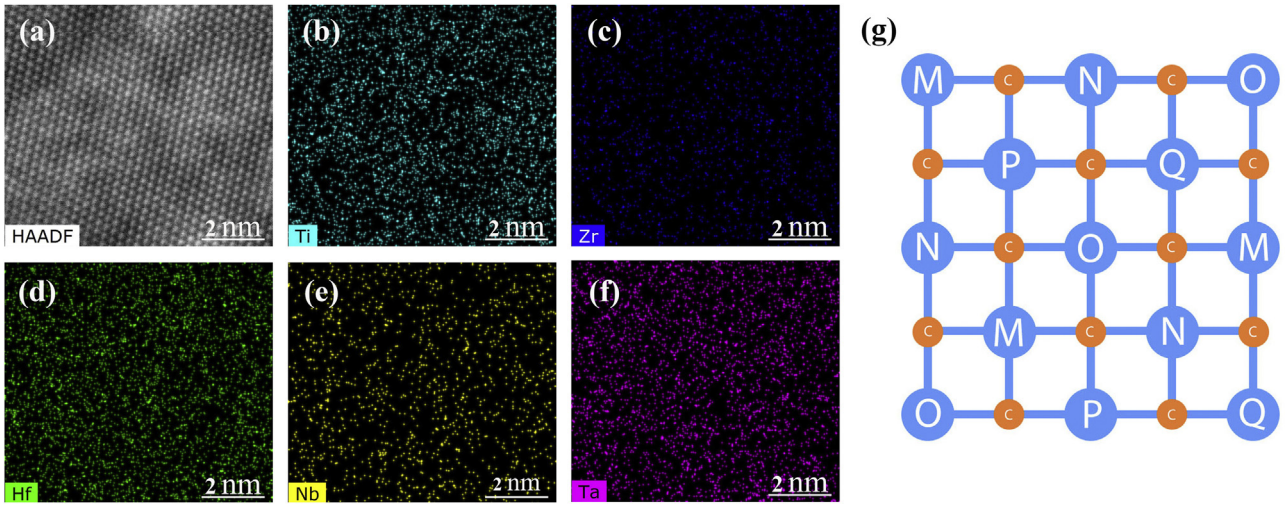

Fig. 2. STEM-EDS analysis of HEC powder. (a) HAADF image. (b-f) Panels labelled as Ti, Zr, Hf, Nb and Ta are intensity maps for the respective characteristic X-rays. The individual EDS maps show uniform spatial distributions for each element and are atomically resolved. (g) Schematic diagram of a cation sublattice co-populated by five metallic ions.

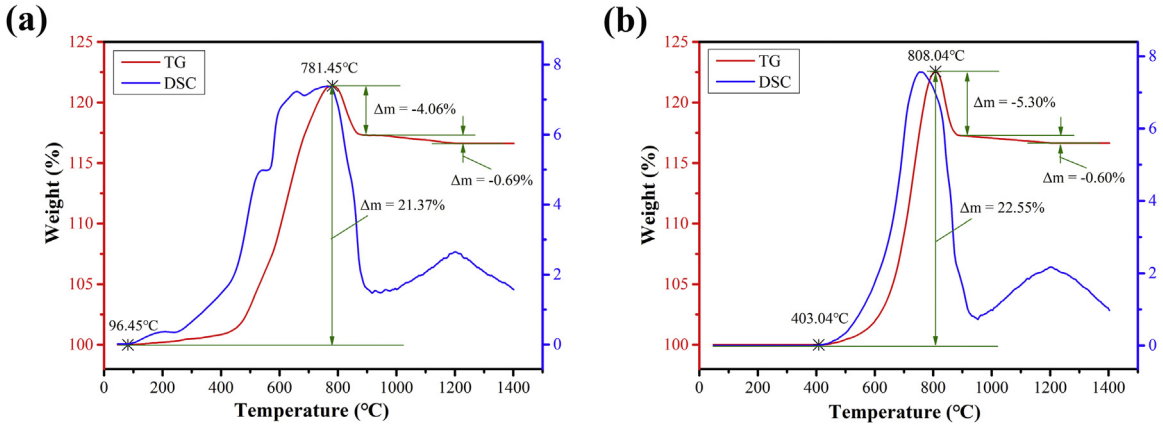

Fig. 3. TG-DSC curves of (a) Mixed powder (b) HEC Powder.

thermogravimetric–differential scanning calorimetry (TG–DSC) analysis was performed. As shown in Fig. 3, obvious differences existed between the oxidation processes of the two samples.

For Mixed powder, the onset of the oxidation occurred at about 96.45 °C. With the increase in temperature beyond 450 °C, the weight gain shows a significant increase and reaches the maximum value at about 781.45 °C. In comparison, the onset of oxidation for HEC powder occurred at about 403.04 °C. The weight gain increased significantly beyond 600 °C and reached its maximum at about 808.04 °C. These differences revealed that the as-prepared HEC powder exhibited a better oxidation resistance than its original components.

Besides, several 'platforms' occurred in the DSC curve of Mixed powder before peaking, indicating that this staged oxidation behaviour in the corresponding temperature range was substantially the combination of separate oxidation processes of its individual components. On the other hand, there only existed one peak with smooth profile in the DSC curve of HEC powder, which means that it acted as an indivisible entirety when undergoing oxidation under relatively lower temperatures.

Therefore, based on previous studies [20–29] and the results obtained in this work, it can be concluded that the following reactions took place during the oxidation process of Mixed powder before peaking.

$$MC + O_2 \rightarrow MO_2 + C\ (M = Ti,\ Zr, Hf) \quad (1)$$

$$PC + x/2O_2 \rightarrow PO_x + C(P = Nb,\ Ta\ 2 < x < 2.5) \quad (2)$$

$$C + O_2 \rightarrow CO_2 \quad (3)$$

Additionally, the possible oxidation mechanism of HEC powder within the same temperature range could be described using Eqs. (4) and (5).

$$(Ti, Zr, Hf, Nb, Ta)\ C + y/2O_2 \rightarrow (Ti, Zr, Hf, Nb, Ta)O_y + C\ (2 < y < 2.2) \quad (4)$$

$$C + O_2 \rightarrow CO_2 \quad (5)$$

Despite these differences, there existed significant similarity between the oxidation behaviours of HEC and Mixed powder after peaking. For both the samples, a small weight loss step and a relatively weak exothermal peak can also be observed between the temperature range of 900–1200 °C, which may be due to the oxidation of a small amount of residual carbon in the samples. Beyond 1200 °C, the weight gain remained almost constant. The similar oxidation behaviour after peaking and the close net weight gain of the two samples suggested that their final oxidation products might almost be the same in composition.

In order to verify the above conjecture, the phase compositions of the oxidation products under different temperature were analysed using XRD and the results are shown in Fig. 4.

From Fig. 4a and b, it can be seen that Mixed powder has been oxidized at 200 °C, while the slight oxidation of HEC powder does not

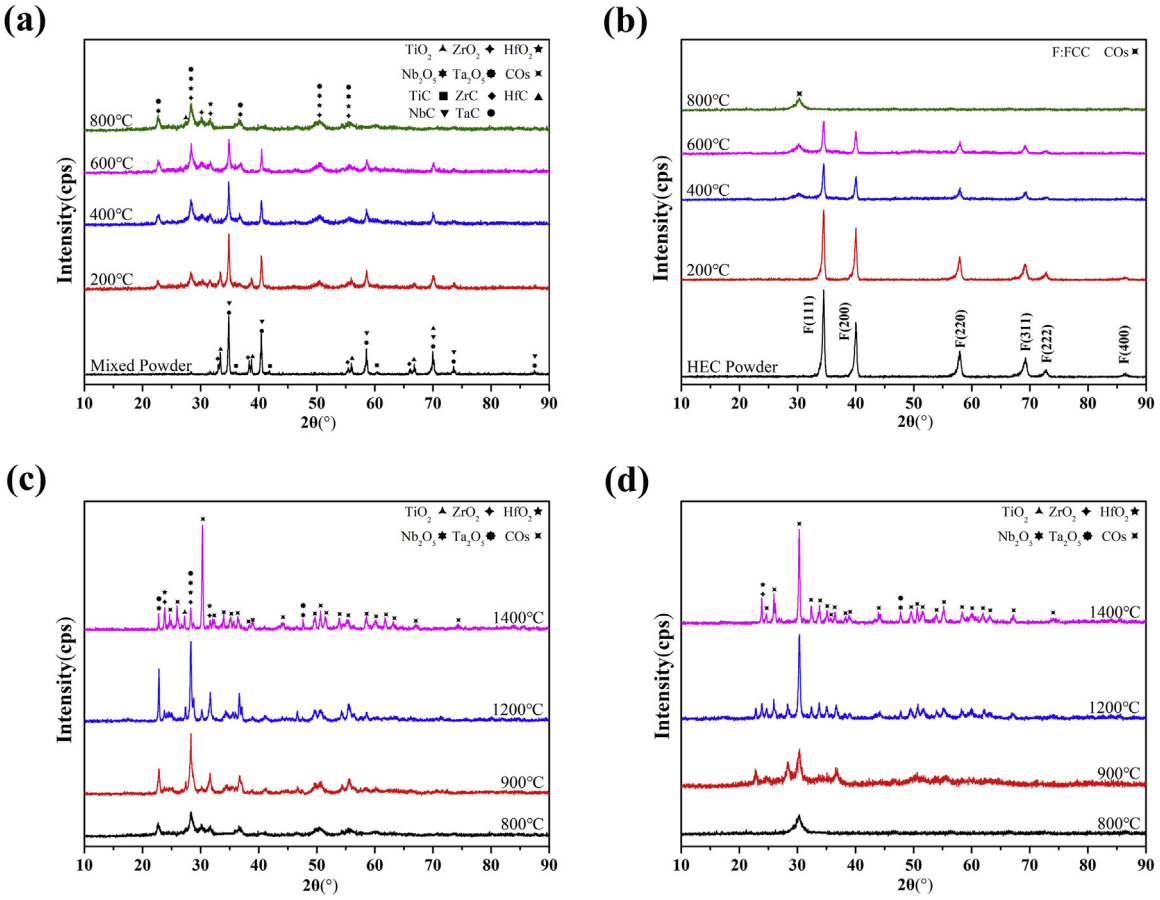

Fig. 4. XRD patterns of the oxidation products of (a) Mixed powder from 200 °C to 800 °C (b) HEC powder from 200 °C to 800 °C (c) Mixed powder from 800 °C to 1400 °C (d) HEC powder from 800 °C to 1400 °C.

happen until 400 °C, which is in accordance with the difference in the onset temperatures of oxidation, as obtained from the TG analysis. In addition, a clear step-by-step oxidation trend of Mixed powder can be seen within the temperature range of 200–800 °C from the XRD results, indicating that its five original components were oxidized separately with the increase in temperature. However, the HEC powder behaved differently while undergoing oxidation and tended to form a single-phase substance having poor crystallinity for the temperature higher than 800 °C. This difference in oxidation processes was in accordance with the DSC results and validates the aforementioned hypothesis on the oxidation mechanism.

With the increase in temperature from 800 °C to 1400 °C, the oxidation of Mixed powder was gradually intensified, as shown in Fig. 4c and d. On the contrary, the oxidation product of HEC powder underwent a decomposition process at the same time, in which the metal oxides of Groups IV B and V B got separated from the quasi-amorphous substance. For both the samples, it should also be pointed out that a certain amount of complex oxides (referred to as COs) was formed due to the reaction among metal oxides of Groups IV B and V B. The oxidation products of both the samples at 1400 °C exhibited significant similarity in phase composition, confirming the hypothesis of similar end-products derived from the TG-DSC analysis.

Both the TG-DSC and XRD results indicated that HEC powder, compared with its original components, exhibited a better performance in terms of oxidation resistance and showed a distinct oxidation process under lower temperatures, which also reflected from the side that HEC powder had relatively high thermal stability.

4. Conclusions

In this work, single-phase, high-entropy ceramics (HEC) consisting of transitional metals in equi-atomic amounts were successfully synthesized using spark plasma sintering. Based upon the results, following conclusions are drawn regarding the properties of HEC.

(1) (Ti, Zr, Hf, Nb, Ta) C HEC was successfully synthesized as a chemically and structurally homogeneous material with the metallic atoms randomly placed within the metallic sublattice.
(2) HEC powder exhibited a better performance in terms of oxidation resistance than its original components and acted as an indivisible entirety while undergoing oxidation under relatively lower temperatures, which reflected from the side that HEC powder had relatively high thermal stability.

The findings verified that the high-entropy theory offered an orthogonal strategy in designing novel phases and uncovering homogeneous crystalline substances. It can be said that this novel theory is opening a thoroughly new research domain in material science and engineering.

Acknowledgments

This work was financially supported by the National Natural Science Foundation of China (51502220, 51521001, 51672197), the Ministry of Science and Technology of China (2015DFR50650), the Self-determined and Innovative Research Funds of WUT (2017II17XZ), and the Open Project Program of Key Laboratory of Inorganic Functional Materials and Devices, Chinese Academy of Sciences (Grant No.:

KLIFMD201606). Useful suggestions given by G. Wei are also acknowledged.

References

[1] J.W. Yeh, S.J. Lin, T.S. Chin, J.Y. Gan, S.K. Chen, T.T. Shun, C.H. Tsau, S.Y. Chou, Formation of simple crystal structures in Cu-Co-Ni-Cr-Al-Fe-Ti-V alloys with multiprincipal metallic elements, Metall. Mater. Trans. A 35 (8) (2004) 2533–2536.

[2] B. Cantor, I.T.H. Chang, P. Knight, A.J.B. Vincent, Microstructural development in equiatomic multicomponent alloys, Mater. Sci. Eng. A 375–377 (2004) 213–218.

[3] P.K. Huang, J.W. Yeh, T.T. Shun, S.K. Chen, Multi-principal-element alloys with improved oxidation and wear resistance for thermal spray coating, Adv. Eng. Mater. 6 (12) (2004) 74–78.

[4] S.K. Chen, C.J. Tong, J.W. Yeh, T.T. Shun, C.H. Tsau, S.J. Lin, S.Y. Chang, Microstructure characterization of AlXCoCrCuFeNi high-entropy alloy system with multiprincipal elements, Metall. Mater. Trans. A 36A (2005) 881–893.

[5] J.W. Yeh, Recent progress in high-entropy alloys, Ann. Chim. Sci. Mater. 31 (6) (2006) 633–648.

[6] A.L. Greer, Confusion by design, Nature 366 (6453) (1993) 303–304.

[7] Y. Zhang, T.T. Zuo, Z. Tang, M.C. Gao, K.A. Dahmen, P.K. Liaw, Z.P. Lu, Microstructures and properties of high-entropy alloys, Prog. Mater. Sci. 61 (2014) 1–93.

[8] M.H. Tsai, J.W. Yeh, High-entropy alloys: a critical review, Mater. Res. Lett. 2 (3) (2014) 107–123.

[9] S.K. Chen, J.W. Yeh, S.J. Lin, J.Y. Gan, T.S. Chin, T.T. Shun, C.H. Tsau, S.Y. Chang, Nanostructured high-entropy alloys with multiple principal elements-novel alloy design concepts and outcomes, Adv. Eng. Mater. 6 (5) (2004) 299–303.

[10] V. Braic, A. Vladescu, M. Balaceanu, C.R. Luculescu, M. Braic, Nanostructured multi-element (TiZrNbHfTa)N and (TiZrNbHfTa)C hard coatings, Surf. Coat. Technol. 211 (2012) 117–121.

[11] J.W. Yeh, B.S. Murty, S. Ranganathan, High-entropy Alloys, Butterworth-Heinemann, London, 2014.

[12] Y. Zhang, Y.J. Zhou, J.P. Lin, G.L. Chen, P.K. Liaw, Solid-solution phase formation rules for multi-component alloys, Adv. Eng. Mater. 10 (6) (2008) 534–538.

[13] W. Ji, Z. Fu, W. Wang, H. Wang, J. Zhang, Y. Wang, F. Zhang, Mechanical alloying synthesis and spark plasma sintering consolidation of CoCrFeNiAl high-entropy alloy, J. Alloy. Compd. 589 (2014) 61–66.

[14] Y.Y. Chen, T. Duval, U.D. Hung, J.W. Yeh, H.C. Shih, Microstructure and electrochemical properties of high entropy alloys—a comparison with type-304 stainless steel, Corros. Sci. 47 (9) (2005) 2257–2279.

[15] C.M. Rost, E. Sachet, T. Borman, A. Moballegh, E.C. Dickey, D. Hou, J.L. Jones, S. Curtarolo, J.P. Maria, Entropy-stabilized oxides, Nat. Commun. 6 (2015) 8485.

[16] D. Bérardan, S. Franger, D. Dragoe, A.K. Meena, N. Dragoe, Colossal dielectric constant in high entropy oxides, Phys. Status Solidi A (RRL) - Rapid Res. Lett. 10 (4) (2016) 328–333.

[17] D. Bérardan, S. Franger, A.K. Meena, N. Dragoe, Room temperature lithium superionic conductivity in high entropy oxides, J. Mater. Chem. A 4 (24) (2016) 9536–9541.

[18] A. Sarkar, R. Djenadic, N.J. Usharani, K.P. Sanghvi, V.S.K. Chakravadhanula, A.S. Gandhi, H. Hahn, S.S. Bhattacharya, Nanocrystalline multicomponent entropy stabilised transition metal oxides, J. Eur. Ceram. Soc. 37 (2) (2017) 747–754.

[19] J. Gild J, Y. Zhang, T. Harrington, et al., High-entropy metal diborides : a new class of high-entropy materials and a new type of ultrahigh temperature ceramics, Sci. Rep. 6 (2016) 37946.

[20] S. Shimada, M. Kozeki, Oxidation of TiC at low temperatures, J. Mater. Sci. 27 (7) (1992) 1869–1875.

[21] S. Shimada, T. Ishil, Oxidation kinetics of zirconium carbide at relatively low temperatures, J. Am. Ceram. Soc. 73 (10) (1990) 2804–2808.

[22] S. Shimada, M. Nishisako, M. Inagaki, et al., Formation and microstructure of carbon-containing oxide scales by oxidation of single crystals of zirconium carbide, J. Am. Ceram. Soc. 78 (1) (1995) 41–48.

[23] S. Shimada, M. Inagaki, K. Matsui, Oxidation kinetics of Hafnium Carbide in the Temperature Range of 480-600 °C, J. Am. Ceram. Soc. 75 (10) (1992) 2671–2678.

[24] S. Shimada, F. Yunazar, S. Otani, Oxidation of hafnium carbide and titanium carbide single crystals with the formation of carbon at high temperatures and low oxygen pressures, J. Am. Ceram. Soc. 83 (4) (2000) 721–728.

[25] S. Shiro, N. Kenichiro, I. Michio, Oxidation of single crystals of hafnium carbide in a temperature range of 600° to 900 °C, J. Am. Ceram. Soc. 80 (7) (2010) 1749–1756.

[26] S. Shimada, A kinetic and thermoanalytical study on oxidation of powder and single-crystal samples of niobium carbide, Oxid. Met. 42 (5–6) (1994) 357–373.

[27] C.F. Miller, G.W. Simmons, R.P. Wei, High temperature oxidation of Nb, NbC and Ni3Nb and oxygen enhanced crack growth, Scr. Mater. 42 (3) (2000) 227–232.

[28] M. Desmaison-Brut, N. Alexandre, J. Desmaison, Comparison of the oxidation behaviour of two dense hot isostatically pressed tantalum carbide (TaC and Ta2C) Materials, J. Eur. Ceram. Soc. 17 (11) (1997) 1325–1334.

[29] S. Shimada, Interfacial reaction on oxidation of carbides with formation of carbon, Solid State Ion. 141–142 (1) (2001) 99–104.